*Technical Note*

# Annual Dynamics of Shortwave Radiation as Consequence of Smoothing Previously Plowed Bare Arable Land Surface in Europe

**Jerzy Cierniewski \* and Jakub Ceglarek** 🆔

Department of Remote Sensing of Environment and Soil Science, Adam Mickiewicz University, Bogumiła Krygowskiego 10, 61-680 Poznan, Poland; jakub.ceglarek@amu.edu.pl
\* Correspondence: ciernje@amu.edu.pl; Tel.: +48-61-8296234

**Abstract:** This paper quantifies the annual dynamics of the shortwave radiation reflected from bare arable land as a result of smoothing previously plowed land located in three different agricultural subregions of the European Union and associated countries. This estimate takes into account the annual variation of the bare arable land area, obtained from Sentinel 2 satellite imagery; the spatial variability of soil units within croplands, obtained from digital soil and land-cover maps; and the laboratory spectral reflectance characteristics of these units, obtained from soil samples stored in the LUCAS soil database. The properties of the soil units, which cover an area of at least 4% of each subregion, were characterized. The highest amounts of shortwave radiation reflected under clear-sky conditions from air-dried, bare arable land surfaces—approximately 850 PJ day$^{-1}$ and 1.10 EJ day$^{-1}$ for land shaped by a plow (Pd) and smoothing harrow (Hs), respectively—were found in the summer around 8 August in the western subregion. However, the lowest radiation occurred in the spring on 10 April at 340 PJ day$^{-1}$ for Pd and 430 PJ day$^{-1}$ for Hs in the central subregion. The largest and the smallest amounts of this radiation throughout the year—only as a result of smoothing, by Hs, land that was previously treated by Pd—was estimated at 42 EJ for the western and southern subregions and 19 EJ for the central subregion, respectively.

**Keywords:** annual variation; shortwave radiation; bare arable lands; hyperspectral reflectance; Sentinel; soil roughness

## 1. Introduction

Although most arable land remains uncovered by vegetation for only a few to several dozen days a year, it is an important component of the Earth's land surface during this period due to its relatively large total area. Arable land covers 13% of the world's land area and as much as 25% of Europe [1]. The land can significantly affect the transfer of energy between soil, vegetation, and the atmosphere. Bare land is a substance that is opaque to shortwave radiation; it does not transmit ($\tau$) it, but only absorbs ($\beta$) and reflects ($\rho$) it. The ratio of this reflected $\rho$ part of solar radiation from bare arable land ($\rho = \psi - \beta$) to the total amount incident on it ($\psi$), expressed as broadband blue-sky albedo ($\alpha = \rho/\psi$), depends on the specific time-stable soil properties characterizing the land, as well as the conditions under which the radiation reaches it. These properties depend primarily on the soil's content of organic carbon (SOC), iron oxides ($Fe_2O_3$), and calcium carbonate ($CaCO_3$). The higher the content of SOC and $Fe_2O_3$, the higher the $\beta = \psi - \rho$ part of the radiation and the lower its $\rho = \psi - \beta$. Consequently, the $\alpha$ value of that soil is lower [2–5]. $CaCO_3$, as a substance conducive to the formation of soil aggregates, increases the roughness of soil surfaces, which increases the $\beta$ part of this radiation, and thus reduces the $\alpha$ value of the soils, although it is very bright. Only when the content of this substance reaches more than 20% do the soils become bright, and their $\alpha$ value increases [6]. The $\alpha$ value of bare soil with specific properties, as mentioned above, may change dynamically due to changes in soil moisture and roughness. Generally,

an increase in soil moisture increases the $\beta$ part of this radiation and reduces the $\rho$ part and, consequently, the overall level of the soil $\alpha$ [7,8]. The soil $\alpha$ decreases significantly as the soil water content increases from hygroscopic capacity to field capacity [9]. Further increasing soil water content to full saturation causes only a slight decrease in the soil $\alpha$ value [10]. Irregularities in the soil surface layer not covered with vegetation, resulting from the presence of soil particles, aggregates, clods, and stones, as well as specific linear micro-relief when shaped by agricultural tools, have a strong impact on the albedo of arable land [11,12]. The $\alpha$ value of bare arable land increases when its irregularities become smaller [13]. Smoothing a deeply plowed arable field using a harrow increases the $\alpha$ by approximately 25% [14]. After heavy rains, when the soil surface has already been air-dried, its $\alpha$ may increase by about 20–30% [15,16]. As a result of the repeated wetting and drying of the top layer of heavy soils, a thin smooth crust is often formed, increasing the $\alpha$ value of such soils by approximately 10–40% [17–19]. The roughness of a bare arable land surface not only determines its overall $\alpha$ level, but also affects the steepness of the $\alpha$ value increase from the solar zenith angle ($q_\mathrm{s}$) at noon solar local time to approximately $q_\mathrm{s} = 75°$. The soil $\alpha$ values of deeply plowed soils remains almost unchanged in this range of $q_\mathrm{s}$, while the $\alpha$ values of the same soils that have been smoothed, for example by using a smoothing harrow, increase significantly in this range [14–16]. The $\alpha$ value of soils under clear-sky conditions changes during the day along with the change in $q_\mathrm{s}$ values. A U-shaped curve is formed, reaching its minimum at noon of local time and its maxima, approaching 1, at sunrise and sunset [20–22]. This shape of the diurnal course of the soil $\alpha$ values is disturbed by the absorption of shortwave radiation by the atmosphere and cloud cover [23]. Generally, diffuse radiation increases with increasing cloud cover, reducing the role of $q_\mathrm{s}$ [24]. Cierniewski et al. [16] proposed a set of equations that can be used to calculate the diurnal albedo variation of bare soils, using 153 sets of soil surface measurements collected in Poland, Israel, and France, representing over 54% of the area of the major soil groups of all arable land in the world. The correctness of these equations, expressed by the coefficient of determination and the mean square error, was estimated at 0.91 and 0.03, respectively. These equations were used to quantify the annual dynamics of shortwave radiation reflected from air-dried, bare arable land treated by agricultural tools in Israel [25,26], the European Union (EU) [26,27], and around the world [28]. Landsat images were used to estimate the annual variation of the bare arable land area in Israel, as well as in Poland [29], using previously formulated equations [15]. However, over a larger area, covering the EU and the whole world, crop calendar datasets were used to estimate the annual variation of bare arable land.

This paper presents the annual dynamics of the amount of shortwave radiation reflected from bare arable land in extremely different roughness states within the EU and its associated countries, in which Sentinel 2 images were used to estimate the variation of the area of bare land to ensure the higher accuracy of such an estimation. The main aim of this paper is to estimate, for large parts of Europe, the annual variation of shortwave radiation, reflected under clear-sky conditions from air-dried, previously deeply plowed arable land surfaces, as a consequence of its smoothing using a smoothing harrow.

## 2. Materials and Methods

### 2.1. Study Area

The study area covers arable land in the European Union, associated countries (Norway, Switzerland), and the United Kingdom (UK) in 2020–2021 (Supplementary Materials). The land was examined within the contours of the 'croplands' category of the analyzed land-cover map in three separate agricultural subregions: western (W), central (C), and southern (S). W includes the croplands of France, Ireland, Portugal, Spain, and the UK; C—Belgium, Denmark, Estonia, Finland, Germany, Latvia, Lithuania, Luxembourg, the Netherlands, Norway, and Sweden; and S—Austria, Bulgaria, Greece, Croatia, Cyprus, Hungary, Italy, Malta, Romania, Slovenia, and Switzerland (Figure 1a). The location of the samples of the main soil groups of the World Reference Base [30] units used to characterize arable land within croplands in each subregion are shown in Figure 1b. The selected

subregions were restricted to the croplands within them (Figure 1b). Soils of arable land were characterized using the main soil groups of World Reference Base (WRB) units, which occupy an area of at least 4% of each subregion (Table 1).
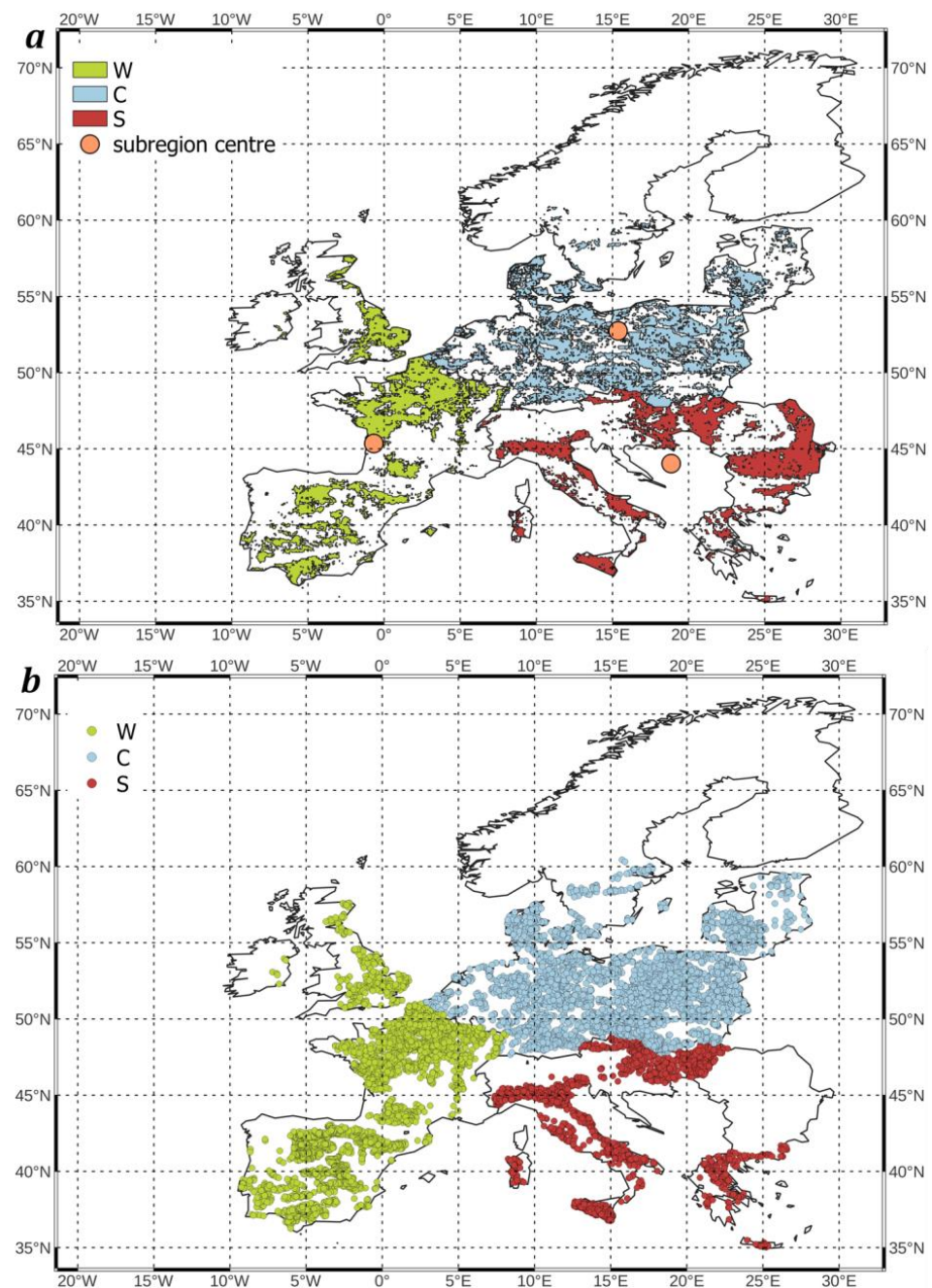


**Figure 1.** Location of: (**a**) 'croplands' contours, according to Modis MODIS/Terra+Aqua Land-Cover Type within the western (W), central (C), and southern (S) subregions; (**b**) the soil samples, from which the main soil groups of the WRB units were used to characterize arable land within croplands of each subregion.

**Table 1.** Areas and numbers of all soil samples, collected from those studied.

| Soil Unit | W | | | C | | | S | | |
|---|---|---|---|---|---|---|---|---|---|
| | Area (10³ km²) | % of W Area | Number of Samples | Area (10³ km²) | % of C Area | Number of Samples | Area (10³ km²) | % of S Area | Number of Samples |
| *Arenosol* | N/A | N/A | N/A | 19.2 | 4.6 | 83 | N/A | N/A | N/A |
| *Cambisol* | 166.4 | 50.5 | 1469 | 110.5 | 26.7 | 615 | 82.9 | 29.6 | 517 |
| *Chernozem* | N/A | N/A | N/A | N/A | N/A | N/A | 51.9 | 18.6 | 122 |
| *Fluvisol* | 31.9 | 9.7 | 260 | 28.2 | 6.8 | 193 | 31.2 | 11.2 | 102 |
| *Gleysol* | N/A | N/A | N/A | 25.7 | 6.2 | 106 | N/A | N/A | N/A |
| *Leptosol* | 24.4 | 7.4 | 242 | N/A | N/A | N/A | N/A | N/A | N/A |
| *Luvisol* | 61.8 | 18.8 | 558 | 125.1 | 30.2 | 650 | 41.6 | 14.9 | 169 |
| *Phaeozem* | N/A | N/A | N/A | N/A | N/A | N/A | 32.8 | 11.7 | 111 |
| *Podzol* | 13.3 | 4.0 | 23 | 61.9 | 15.0 | 340 | 12.4 | 4.4 | 2 |
| *Vertisol* | N/A | N/A | N/A | N/A | N/A | N/A | 16.4 | 5.8 | 38 |
| Sum | | 90.4 | 2552 | | 89.5 | 1987 | | 91.8 | 1061 |

### 2.2. Bare Arable Land Area

The following procedure was conducted for each country grouped within the selected subregions. First, the croplands class from the MODIS/Terra+Aqua Land-Cover Type dataset [31] was selected, and everything not belonging to the croplands class was masked out and omitted from further analysis. The occurrences of bare soil were found using Sentinel 2 imagery. This procedure was performed in Google Earth Engine [32]. First, the period of analysis was set from 23 December 2020 to 22 December 2021 and divided into 10-day periods. For each one, Sentinel 2 imagery, covering areas of the croplands within each subregion, was obtained. The pixels that were marked as opaque, or those that contained cirrus clouds using the Sentinel quality band (QA), were masked. From all the filtered pixels, a cloudless mosaic was composed for each 10-day period; the mean value was used if more than one unmasked pixel was found for any given period. The bare soils were identified using the modified formula, found in the previous work [29], with the different band numbers due to the switch from Landsat 9 to Sentinel 2 data. Next, for a pixel to be classified as bare arable land, both of the following conditions had to be met:

$$B2 < B3 < B4 < B8 < B11 > B12 \text{ and } B8/B3 > 1.5,$$

where each term refers to the reflectance in Sentinel 2 band with its corresponding number. The presented conditions are based on the shape of the spectral curve of soils and were previously tested on the example of the Landsat bands [29]. This procedure outputted binary maps, separating bare arable land and vegetation within the contours of croplands. The areas of bare land were calculated by summing all eligible pixels. This operation was performed for each 10-day period of the tested year–plotting the annual variation of bare land area first in this function. Finally, by smoothing its course, it was obtained as a function of subsequent days of the year (DOYs).

### 2.3. Diurnal Albedo of the Land

Spectral properties of the land were described using reflectance spectra of the main groups of World Reference Base for Soil Resources (WRB) units. These spectra, in the 350–2500 nm range, relating to soil samples located within these units, were obtained from the Land Use and Coverage Area-Frame Survey (LUCAS) [33]. Additionally, data characterizing the properties of these units were downloaded from this database: soil texture, SOC and $CaCO_3$ content; these significantly affect reflectance in the shortwave radiation range. These data made it possible to characterize the spatial variation of soils in the studied subregions. These obtained spectra were weighted according to a previously measured share of area for each unit within the subregions. Then, the averaged spectra

of the land in these three subregions were used to predict their mean diurnal albedo values ($a_d$) during the studied period using custom SALBEC software, version 0.9a [34]; it was assumed that the surfaces were shaped by plows (Pd) and smoothing harrows (Hs). Additionally, the following data, defined as input data, were used for each tested surface:

- the location of the studied surfaces (latitude and longitude in decimal degree format)
- the date range to be used for calculating the $a_d$ values of the studied surfaces
- two roughness indices, namely the standard deviation of their surface height (HSD) and the index, defined as the ratio of the actual surface within the basic unit to its flat horizontal surface ($T_{3D}$)

As in the previous paper [29], the following values of these roughness indices for surfaces shaped by Pd and Hs were used: respectively, 25 and 5 mm (for HSD) and 1.5 and 1.05 (for $T_{3D}$). SALBEC uses four equations to calculate the diurnal variation in the $\alpha$ value of a soil surface with a specific roughness. The first equation [16]:

$$a_{45} = 0.33 - 0.1099T_{3D} - 5795.4d_{574} - 510.2d_{1087} + 7787.2d_{1355} + 12161d_{1656} + 6932.8d_{698} , \tag{1}$$

computes the overall $a$ level of the surface at $\theta_s = 45°$ ($a_{45}$), where $d$, together with its associated number relates to the soil reflectance data transformed to the second derivative for a specified wavelength in nm. The second equation [16]

$$\alpha_{\theta_s} = \alpha_{45}[1 + s_\alpha(\theta_s - 45)], \; s_\alpha = 6.26 \times 10^{-7} + 0.0043 \, (HSD)^{-1.418} \tag{2}$$

computes the $\alpha$ values of the tested surface ($a_{\theta s}$) below $\theta_s < 75\,°$, where $s_a$ is the slope of the $a$ rise. The third equation [16]

$$\alpha_{\theta_s} = exp\left(\frac{a + c\theta_s}{1 + b\theta_s + d(\theta_s)^2}\right) \tag{3}$$

enables one to fit the course of the relations between $\alpha$ of the soil surface and the $\theta_s$ for the $\theta_s$ range from 0° to 90°. This relationship is complemented by $\alpha = 1$ when $\theta_s = 90°$ and where symbols $a$, $b$, $c$, and $d$ denote the fitted parameters of the equation. The fourth equation [34]

$$\alpha_d = \frac{1}{|L|} \cdot \Sigma\alpha_d \tag{4}$$

allows the $a_d$ value to be calculated by transforming Equation (3) into the integral, where $L$ denotes the length of the $a_{\theta s}$ list.

### 2.4. Shortwave Radiation of the Land

To calculate shortwave radiation reflected from the land formed by the Hs and Pd, the annual variation of the incoming radiation in clear-sky conditions was calculated based on the equation proposed by Allen et al. [35]. The diurnal albedo patterns of the surfaces, representing the studied subregions, were converted to solar local time throughout the year at the subregion centers. The annual variation of the amount of radiation reflected from the land in clear-sky conditions was obtained by multiplying the amount of the radiation incident upon the land with its mean diurnal albedo values, related to a farming practice, by the area of the bare land for any given DOY. Then, the increase of the reflected radiation resulting from the smoothing, by Hs, of the surfaces previously treated by Pd, was the difference between the radiation reflected from those surfaces. The total annual amount of the reflected radiance and the difference was calculated by integrating the areas under the related curves.

## 3. Results

### 3.1. Soil Units of the Land

It was determined that the areas of the contours of the croplands category on the analyzed land-cover map within three agricultural subregions—W, C, and S—are approximately 329, 414, and 280 thousand square kilometers, respectively (Figure 1a). Properties of soils located within these contours (belonging to specific main groups of WRB soil units) that significantly affect their reflectance in the range of shortwave radiation were obtained from data describing over 2550, almost 1990, and over 1060 soil samples collected in W, C, and S, respectively (Table 1). Table 1 contains data on these units, which together cover at least 90% of the area of each of the studied subregions. Cambisols and Luvisols together have the largest shares in each of these subregions: 50% and 19% in W, 27% and 30% in C, and 30% and 15% in S. Cambisols, developed from loam (L) in W and C and clay loam (CL) in S, have, on average, a similar SOC content of 1.6% in W and S, but its content of 2.2% is clearly higher in C (Table 2).

**Table 2.** Average properties: Texture and contents of sand, silt and clay, soil organic carbon (SOC), carbonates (CaCO$_3$)of the WRB soil units within the 'croplands' category of each subregion—western (W), central (C), and southern (S). Texture is presented with respect to types in Soil Survey Staff (1975): sandy loam (SL), loam (L), silty loam (SiL), clay loam (CL), and silty clay loam (SiCL).

| Soil Unit | W Sand (%) | W Silt (%) | W Clay (%) | W Texture | W SOC (%) | W CaCO$_3$ (%) | C Sand (%) | C Silt (%) | C Clay (%) | C Texture | C SOC (%) | C CaCO$_3$ (%) | S Sand (%) | S Silt (%) | S Clay (%) | S Texture | S SOC (%) | S CaCO$_3$ (%) |
|---|---|---|---|---|---|---|---|---|---|---|---|---|---|---|---|---|---|---|
| *Arenosol* | N/A | N/A | N/A | N/A | N/A | N/A | 70.9 | 22.3 | 6.8 | SL | 1.27 | 0.27 | N/A | N/A | N/A | N/A | N/A | N/A |
| *Cambisol* | 30.4 | 43.8 | 25.8 | L | 1.64 | 14.82 | 40.4 | 38.3 | 21.3 | L | 2.19 | 1.20 | 27.5 | 45.2 | 27.3 | CL | 1.63 | 9.20 |
| *Chernozem* | N/A | N/A | N/A | N/A | N/A | N/A | N/A | N/A | N/A | N/A | N/A | N/A | 20.9 | 53.6 | 25.5 | SiL | 1.97 | 4.77 |
| *Fluvisol* | 36.5 | 41.1 | 22.4 | L | 1.46 | 10.78 | 43.2 | 39.3 | 17.5 | L | 1.63 | 2.71 | 26.8 | 46.0 | 27.2 | CL | 1.59 | 6.09 |
| *Gleysol* | N/A | N/A | N/A | N/A | N/A | N/A | 50.5 | 35.4 | 14.1 | SL | 2.43 | 0.85 | N/A | N/A | N/A | N/A | N/A | N/A |
| *Leptosol* | 23.6 | 49.0 | 27.4 | CL | 2.1 | 26.78 | N/A | N/A | N/A | N/A | N/A | N/A | N/A | N/A | N/A | N/A | N/A | N/A |
| *Luvisol* | 32.0 | 47.3 | 20.7 | L | 1.51 | 2.2.8 | 46.7 | 40.6 | 12.7 | L | 1.46 | 0.77 | 25.2 | 52.5 | 22.3 | SiL | 1.43 | 0.85 |
| *Phaeozem* | N/A | N/A | N/A | N/A | N/A | N/A | N/A | N/A | N/A | N/A | N/A | N/A | 17.8 | 51.2 | 31.0 | SiCL | 2.03 | 3.71 |
| *Podzol* | 59.1 | 30.5 | 10.3 | SL | 2.69 | 0.47 | 61.8 | 27.0 | 11.2 | SL | 3.33 | 0.11 | 51.0 | 33.0 | 16.0 | L | 3.08 | 0.15 |
| *Vertisol* | N/A | N/A | N/A | N/A | N/A | N/A | N/A | N/A | N/A | N/A | N/A | N/A | 19.5 | 43.1 | 37.4 | SiCL | 1.61 | 2.52 |

The SOC content of Luvisols in all subregions is about 15%. The average CaCO$_3$ content in Cambisols located in W exceeds 15%, while in C and S, it reaches only 1.2% and 0.9%, respectively. The average CaCO$_3$ content of Luvisols in W, is 2.3%, which is higher than in C and S, where it does not exceed 1%. Fluvisols, developed from L in W and C, cover approximately 10% of W and 7% of C. The SOC content of their average unit is quite similar to that determined for Cambisols and Luvisols. The CaCO$_3$ content of Fluvisols, developed from L in W, is 11%—clearly higher than in C and S, where, being developed from L and CL, it reaches 2.7% and 6.1%, respectively.

The SOC contents in W, C, and S are between 1.5% and 1.6%. Podzols, developed from sandy loam (SL) in W and C and from L in S, which occupies 15% of the C area and only about 4% of the W and S areas. Their averaged units in W, C, and S reach SOC contents of 2.7%, 3.3%, and 3.1%, respectively, and lower CaCO$_3$ contents of approximately 0.5%, 0.1%, and 0.2%, respectively. Leptosols, developed from CL, occupy over 7% of the W area. Their average unit is characterized by a very high CaCO$_3$ content of 27% and a relatively high, about 2%, SOC content. Gleysols, developed from sandy loam (SL), occur on about 6% of the C area. Its average unit has a relatively high SOC content, about 2%, and a low CaCO$_3$ content, about 0.8%. Arenosols, found only in C, cover almost 5% of its area. Their average unit is characterized by very similar properties to those determined for Leptosols.

Chernozems and Phaeozems, developed from silty loam (SiL) and silty clay loam (SiCL), respectively, are found only in S, and occupy nearly 19% and 12% of their areas, respectively. Their average units have a high SOC content of 2.0% in both cases, and also a high CaCO$_3$ content of 4.8% and 3.7% in these first and second units, respectively.

Fluvisols within S, developed from CL, cover 11% of its area. Their average unit contains approximately 1.6% SOC and 6% CaCO$_3$. Vertisols, found only in C, developed there from SiCL and occupy only 6% of its area. Their average unit contains over 1.6% SOC and 2.5% CaCO$_3$.

### 3.2. Shortwave Radiation of the Land

The greatest diversity of the reflectance spectra of soil samples for soil units collected within the studied subregions, was found in the S subregion. The lowest reflectance was determined for the dark-colored Phaeozems and Chernozems, developed there from SICL and SIL, with a relatively high average SOC content (about 2%) and a relatively high (4–5%) average CaCO$_3$ content, which, at these levels, contribute to increasing the roughness of their surfaces (Figure 2). Meanwhile, the lowest reflectance was determined for light-colored Cambisols, developed from CL, covering almost one third of the surface of this subregion, with a low average SOC content (about 1.5%), but the highest average CaCO$_3$ content (over 9%) among the analyzed soil units, which, however, should not increase the reflectance of these soils (Table 2). The smallest difference in reflectance can be seen between the main groups in W, where the spectra of two large-area soil units (Cambisols and Luvisols) are characterized by the similar average (approximately 1.5%) SOC content.
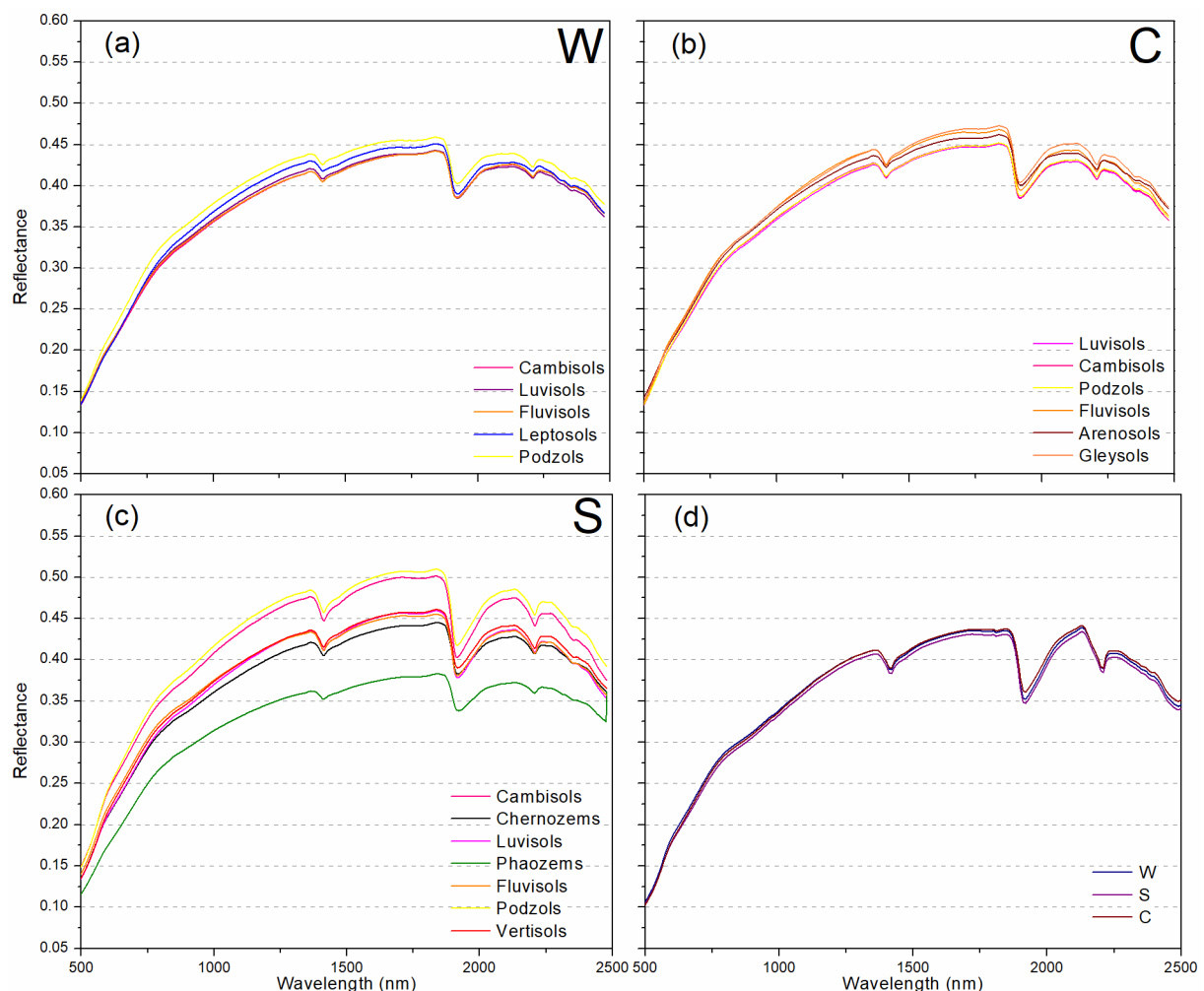


**Figure 2.** Reflectance spectra of the studied soil units: (**a–c**), averaged for the units in the western (W), central (C), and southern (S) subregions; (**d**), averaged for all the units located within these subregions.

The patterns of three averaged reflectance spectra, calculated separately for the W, C and S subregions from a large number of reflectance spectra (listed at the beginning of

this section), associated with all soil samples taken from individual subregions, are very similar to each other (Figure 2). The maxima of the shortwave radiation amount reaching the studied subregions under clear-sky conditions during the year are approximately 32 TJ km$^{-2}$ day$^{-1}$ in all these regions at the beginning of the astronomical summer on the 173rd day of the year (DOY) (22 June) (Figure 3a). However, the minima of the amounts are expected at the beginning of the astronomical winter on the 356th DOY (22 December). For subregion C, with its center at the highest latitude, 52.7°, the minimum was calculated to be less than 5 TJ km$^{-2}$ day$^{-1}$, while for subregions W and S, located at latitudes 45.3° and 44.0°, respectively, it was 7.5 TJ km$^{-2}$ day$^{-1}$ and 8 TJ km$^{-2}$ day$^{-1}$, respectively.
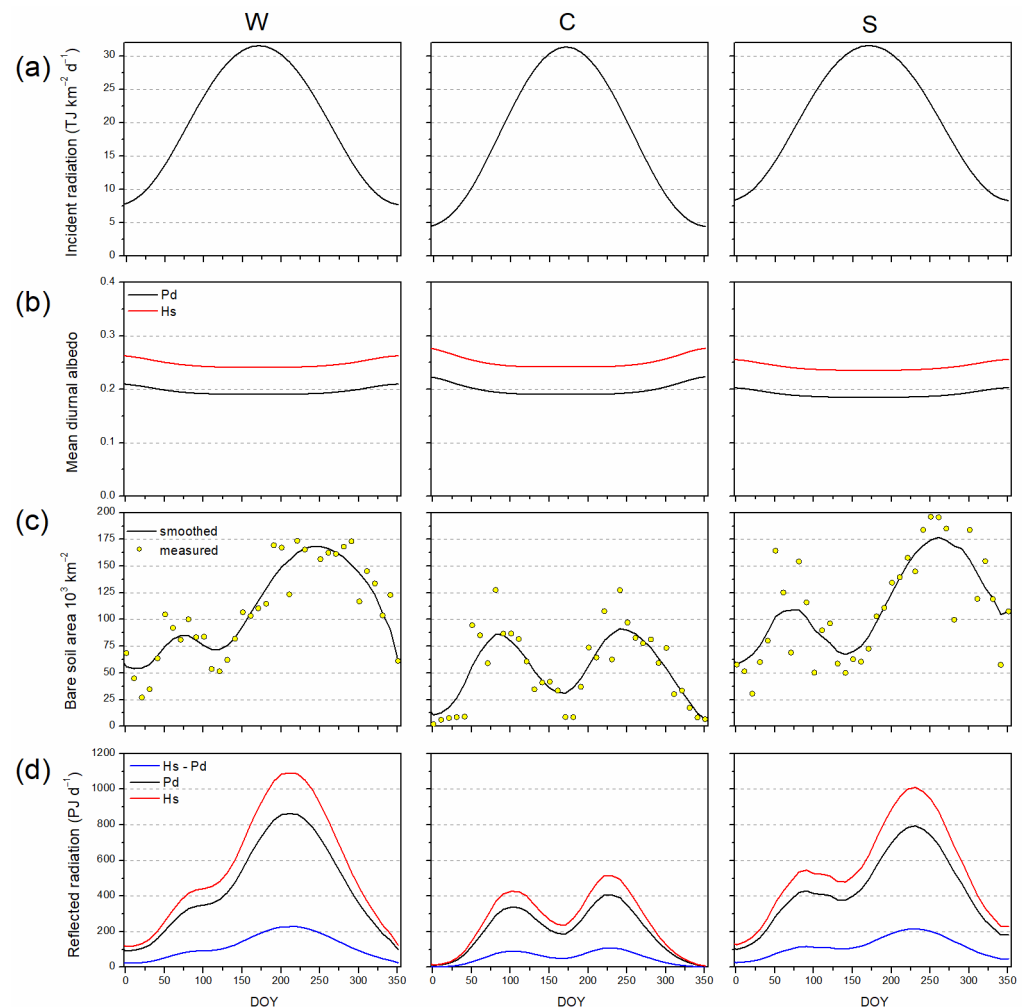


**Figure 3.** Annual variations within analyzed subregions in (**a**) amount of shortwave radiation reaching the land in clear-sky conditions; (**b**) average diurnal blue-sky albedo ($\alpha_d$) of the average air-dried surfaces of bare land formed by a plow (Pd), and smoothing harrow (Hs); (**c**) areas of bare arable land; and (**d**) amount of shortwave radiation reflected under clear-sky conditions from air-dried surfaces of the land shaped by a Pd and Hs and amount of this radiation resulting of smoothing the land by a Hs previously treated Pd. DOY—day of the year.

Contrary to the annual variation of the amount of shortwave radiation reaching the studied subregions under clear-sky conditions, the annual variation of the blue-sky albedo of air-dried arable land surfaces, shaped by Pd and Hs within these subregions, shows its maxima and minima on the 356th DOY and 173rd DOY, respectively (Figure 3b). These extreme minimum and maximum blue-sky albedo values of air-dried, arable land surfaces in the studied subregions are obviously lower for the surfaces shaped by Pd than by Hs (Table 3).

**Table 3.** Minimum and maximum blue-sky albedo values of air-dried, arable land surfaces shaped by a plow (Pd) and smoothing harrow (Hs) on the 173rd day of the year (DOY) and the 356th DOY within the studied subregions–western (W), central (C), and southern (S).

| Sub-Region | Tool | 173rd DOY | 356th DOY |
|---|---|---|---|
| W | Pd | 0.191 | 0.210 |
| | Hs | 0.241 | 0.263 |
| C | Pd | 0.192 | 0.224 |
| | Hs | 0.242 | 0.277 |
| S | Pd | 0.214 | 0.232 |
| | Hs | 0.236 | 0.256 |

In the annual variation of the arable land area within the studied subregions, two increases are clearly visible: smaller ones, occurring at the turn of winter and spring in the period of about 25–150 DOY, and larger ones at the turn of summer and autumn in the period of 125–350 DOY (Figure 3c). This first increase appeared earliest within the S subregion. Its peak occurred on the 75th DOY (16 March), reaching approximately 105,000 km$^2$. The second peak occurred in S on the 250th DOY (7 September), reaching about 175,000 km$^2$. The first increase within the W, on the 75th DOY, reached approximately 82,000 km$^2$, while the second one reached approximately 165,000 km$^2$ on around the 250th DOY. These two increases for subregion C are almost equal in relation to the area at their peaks. This first peak reached about 83,000 km$^2$ on the 80th DOY (21 March) and the second one about 85,000 km$^2$ on the 250th DOY. The annual variation of the amount of shortwave radiation, reflected in clear-sky conditions from air-dried, bare surfaces of arable land shaped by Pd and Hs in the studied subregions, was determined jointly by two different annual courses describing the variation of the blue-sky albedo values of these surfaces (Figure 3b), as well as their area when they are not covered with vegetation (Figure 3c,d). It was found that the greatest amount of shortwave radiation was reflected by bare arable land in the W subregion. This amount, in its second peak that occurred in the summer around 220th DOY (8 August), was determined to be approximately 850 PJ day$^{-1}$ and 1.10 EJ day$^{-1}$ for land shaped by Pd and Hs, respectively. In its first, clearly lower peak, determined in the spring on the 100th DOY (10 April), these amounts were calculated at approximately 350 PJ day$^{-1}$ for Pd and 450 PJ day$^{-1}$ for Hs. The increase in the amount of shortwave radiation resulting from the smoothing, by Hs, of the land previously shaped by Pd, was calculated from the difference in the amount of this radiation for the land shaped by Hs and Pd, respectively, and estimated in this subregion at about 230 PJ day$^{-1}$ in its higher peak and about 80 PJ day$^{-1}$ in the lower one. This total amount of reflected radiation over the entire year from the land shaped by Pd and Hs, added up day by day, was estimated in W to be 158 EJ and 200 EJ, respectively, while the total amount of this radiation reflected during the year as a result of smoothing the land was estimated at 42 EJ. Quite similar amounts of this radiation were determined for the land in the S subregion. In the higher peak, which also occurred in summer, but later, on around the 225th DOY (13 August), this amount was estimated at about 800 PJ day$^{-1}$ for Pd and about 1.0 EJ day$^{-1}$ for Hs. In this lower peak, occurring on the 80th DOY, the amount was determined at 420 PJ day$^{-1}$ for Pd and 530 PJ day$^{-1}$ for Hs. The amount of this radiation, as the result of smoothing the land in this higher and lower peak, was calculated at 210 PJ day$^{-1}$ and 110 PJ day$^{-1}$, respectively. The total amount of this reflected radiation over the entire year from land within S, shaped by Pd and Hs, was estimated at 155 EJ and 196 EJ, respectively. However, the total annual amount of this reflected radiation as the consequence of smoothing the land in this subregion, as in subregion S, was calculated at approximately 42 EJ. In subregion C, the amount of this radiation reflected from the land, shaped by Pd and Hs, was characterized in two similar-sized increases with their peaks occurring there around the 100th DOY and the 230th DOY (18 August). The amount of this radiation in this second, slightly higher peak was estimated at approximately 400 PJ day$^{-1}$ and 520 PJ day$^{-1}$ for the land treated by Pd and Hs, respectively, whereas in the first, slightly lower peak, it was approximately 340 PJ day$^{-1}$ and 430 PJ day$^{-1}$, respectively. With smoothing by Hs, the land previously treated by Pd in this

subregion resulted in an increase in this radiation by approximately 110 PJ day$^{-1}$ in its higher peak and 90 PJ day$^{-1}$ at the lower one. The total amount of this radiation over the entire year, from the land in this subregion shaped by Pd and Hs, was calculated at 91 EJ and 72 EJ, respectively. The total annual amount of this radiation, as a consequence of the smoothing of the land in this subregion, was calculated at 19 EJ.

## 4. Discussion

The procedure used in this study does not allow for the detection of the roughness state of bare arable land, shaped by Pd and smoothed by Hs, based on satellite imagery. Using the relationship between individual bands of the Sentinel 2 satellite, only fragments of arable land that were not covered with vegetation were detected, and the annual variation in their areas in three EU subregions was determined. It is only assumed that this bare land, after deep plowing (using Pd), may be smoothed after some time. We assume that a rapid reduction in the roughness of bare arable land covering large areas of the Earth, even for relatively short periods of the year, may slow down the warming of the Earth's climate, at least on a regional scale. The consequence of reducing the roughness of arable land, and thus increasing the amount of shortwave radiation reflected from its surfaces, is a simultaneous reduction in the amount of this radiation that can be absorbed by the surface layer of such land. This layer becomes cooler and emits less long-wave radiation [36–40]. Deepening research on the relationship between the shortwave radiation reflected and absorbed by bare soil surfaces and the long-wave radiation emitted by them, depending on their roughness, could help to assess the impact of agricultural practices on climate more accurately at regional scales.

This study is based on the actual annual variation of bare arable land areas in 2021 obtained using satellite images in three phenologically different agricultural regions of Europe. The influence of soil texture, SOC, and CaCO$_3$ content was not discussed separately in specific subregions. This was because, after appropriately weighted averaging of the spectra representing individual soil units, it turned out that these averaged spectra (which were the basis for calculating the annual variability of mean diurnal albedo values), in all subregions, differed very little from each other (Figure 2). It was therefore difficult to discuss the influence of soil texture, SOC and CaCO$_3$ using the pattern of such averaged spectra that characterized all analyzed soil units within the studied subregions. Even using the example of the S subregion, where the diversity of the analyzed spectra in relation to the corresponding soil units is the clearest, it was not possible to formulate sufficiently clear correlations between them–probably due to the averages calculated.

This investigation used the spectral features of averaged main groups of soil units rather than selected actual soil units obtained from the LUCAS soil database. Therefore, the obtained results, which refer only to air-dried soil surfaces under clear-sky conditions, are difficult to verify practically.

Soil shortwave reflectance spectra measured in laboratories using standard protocols [41], obtained from tens of thousands of soil samples associated with their location, can be used in similar studies in many other places in the world. These spectra are collected in global soil databases, such as the International Soil Information and Reference Center (ISRIC) [42] or the Global Soil Spectral Library [43].

The patterns of annual variation of the areas of bare arable land in these three subregions, found as a result of this study, differ in their shape and levels from the corresponding patterns in the previously published paper [27]. The patterns in that paper were determined using the crop calendar dataset (created by Sacks et al. [44]), which makes it possible to define the days of the year when arable land becomes bare in the analyzed parts of the world, before sowing and after harvesting major crops, using vectorized and rasterized crop calendars dataset. Two actual increases in the areas of bare arable land during the year in each the studied subregions, the first occurring at the turn of winter and spring and the second at the turn of summer and autumn, were found in almost the same periods as those previously determined using data from crop calendars. However, their peaks, representing

the actual maximum values of bare arable land in these subregions and determined using satellite images, are clearly higher and in different proportions relative to each other than the peaks obtained using crop calendars data.

The almost equal heights of the two peaks that show the actual maximum areas of bare arable land were also found in Poland (covering a significant part of subregion C). They were presented in a previous study [26] and were also determined using satellite images, similar to how the peaks were determined in this study for the entire subregion C in Europe. This confirms that the procedure using satellite images is more reliable than the one using crop calendars data.

The total amounts of shortwave radiation, reflected under clear-sky conditions throughout 2021 from air-dried, bare land surfaces shaped by Pd and Hs in all three studied EU agricultural subregions, were 385 EJ and 487 EJ, respectively, and correspond to more than 38 times and 48 times the amount of electricity produced by all power plants in the EU in the analyzed year (2785 TWh), according to Eurostat [45]. The total annual amount of this radiation in these three subregions, which was only the effect of smoothing the studied land, which was previously shaped by Pd, by Hs (taking into account the above limitations regarding the moisture state of the land and its illumination conditions), estimated at 103 EJ, which corresponds to more than 10 times the production of electricity in the EU in the year under consideration.

## 5. Conclusions

This study quantifies the annual variation of shortwave radiation reflected from bare arable land in three phenologically different agricultural subregions western (W), central (C), and southern (S), of the EU and associated countries, using:

- annual variability of bare arable land areas obtained using Sentinel 2 imagery
- spatial differentiation of the main soil groups of WRB units within the contours of agricultural fields, obtained from digital soil and land cover maps
- annual variability of the average daily albedo of these units, assuming that their surfaces were shaped by a plow (Pd) and a smoothing harrow (Hs), calculated using the specialized SALBEC program on the basis of the reflectance spectra of units stored in the soil LUCAS database

These data allowed us to establish the following results.

Large areas of bare arable land occur in two periods during the year: at the turn of winter and spring and of summer and autumn, presenting the largest areas, of different sizes, in individual subregions in their two peaks.

The greatest amounts of shortwave radiation reflected under clear-sky conditions from air-dried, bare arable land–approximately 850 PJ day$^{-1}$ and 1.10 EJ day$^{-1}$ for the land shaped by Pd and Hs, respectively–were determined in the summer around the 220th day of the year (DOY) (8 August) in W. Also, in summer, around the 225th DOY (13 August), similar amounts of this radiation were predicted for such lands in S, namely about 800 PJ day$^{-1}$ for those shaped by Pd and about 1.0 EJ day$^{-1}$ for those treated by Hs. Also, in summer, around (18 August), these amounts for C were significantly lower, reaching only approximately 400 PJ day$^{-1}$ and 520 PJ day$^{-1}$ for the land treated by Pd and Hs, respectively.

Significantly lower amounts of this radiation—approximately 350 PJ day$^{-1}$ for Pd and 450 PJ day$^{-1}$ for Hs—were determined in the spring on the 100th DOY (10 April) in W, as well as 340 PJ day$^{-1}$ for Pd and 430 PJ day$^{-1}$ for Hs on the same DOY in C, whereas, in S, at the turn of winter and spring, around the 80th DOY (21 March), the amounts of this radiation were higher—approximately 400 PJ day$^{-1}$ and 520 PJ day$^{-1}$ for the land treated by Pd and Hs, respectively.

The largest and the smallest amounts of this reflected radiation throughout the year, only as a result of smoothing land, by Hs, previously treated by Pd, were estimated at 42 EJ for W and S and 19 EJ for C, respectively.

When it is no longer possible to deny the global warming of the Earth's climate, one of the actions that could slow down this warming is to ensure arable land for conventional cultivation has the lowest possible roughness.

## References

1.  World Bank, Arable Land (% of Land Area). Available online: https://data.worldbank.org/indicator/AG.LND.ARBL.ZS (accessed on 10 January 2024).
2.  Al-Abbas, A.H.; Swain, P.H.; Baumgardner, M.F. Relating Organic Matter and Clay Content to the Multispectral Radiance of Soils. *Soil. Sci.* **1972**, *114*, 477–485. [CrossRef]
3.  Bauer, M.E.; Vanderbilt, V.C.; Robinson, B.P.; Daugtry, C.S.T. Spectral Propertis of Agricultural Crops and Soils Measured Space, Aerial. In *Field and Laboratory Sensors*; Purdue University: West Lafayette, IN, USA, 1981.
4.  Białousz, S.; Girard, M.G. Wspolczynniki Odbicia Spectralngo Gleb w Pasmach Pracy Satelity Landsat. *Fotointerpr. Geogr.* **1978**, *3*, 111–117. (In Polish)
5.  White, J.L. Interpretation of Infrared Spectra of Soil Minerals. *Soil Sci.* **1971**, *112*, 22–29. [CrossRef]
6.  Bialousz, S. Zastosowanie Fotointerpretacji Do Wykonywania Map Stosunków Wodnych Gleb. *PTG Pr. Kom. Nauk.* **1978**, *35*, 1–143. (In Polish)
7.  Baumgardner, M.; Silva, L.; Biehl, L.; Stoner, E. Reflectance Properties of Soils. *Adv. Agron.* **1986**, *38*, 1–44.
8.  Idso, S.B.; Jackson, R.D.; Reginato, R.J.; Kimball, B.A.; Nakayama, F.S. The Dependence of Bare Soil Albedo on Soil Water Content. *J. Appl. Meteorol. Climatol.* **1975**, *14*, 109–113. [CrossRef]
9.  Bowers, S.A.; Smith, S.J. Spectrophotometric Determination of Soil Water Content. *Soil Sci. Soc. Am. J.* **1972**, *36*, 978–980. [CrossRef]
10. Cierniewski, J. Soil Moisture Tension and Soil Spectra Reflectance on the Example of Koscian Plain Soils. *Fotointerpr. Geogr.* **1993**, *105*, 107–122.
11. Cierniewski, J. *Geometrical Modeling of Soil Bi-Directional Reflectance in the Optical Domain*; Bogucki Science Publisher: Poznan, Poland, 1999.
12. Cierniewski, J. *The Bidirectional Reflectance Model from Cultivated Soils Taking into Account Soil Aggregates and Micro-Relief*; Bogucki Science Publisher: Poznan, Poland, 2001; p. 150. (In Polish)
13. Matthias, A.D.D.; Fimbres, A.; Sano, E.E.E.; Post, D.F.F.; Accioly, L.; Batchily, A.K.K.; Ferreira, L.G.G. Surface Roughness Effects on Soil Albedo. *Soil Sci. Soc. Am. J.* **2000**, *64*, 1035–1041. [CrossRef]
14. Cierniewski, J.; Karnieli, A.; Kazmierowski, C.; Krolewicz, S.; Piekarczyk, J.; Lewinska, K.; Goldberg, A.; Wesolowski, R.; Orzechowski, M. Effects of Soil Surface Irregularities on the Diurnal Variation of Soil Broadband Blue-Sky Albedo. *IEEE J. Sel. Top Appl. Earth Obs. Remote Sens.* **2015**, *8*, 493–502. [CrossRef]
15. Cierniewski, J.; Ceglarek, J.; Karnieli, A.; Królewicz, S.; Kaźmierowski, C.; Zagajewski, B. Predicting the Diurnal Blue-Sky Albedo of Soils Using Their Laboratory Reflectance Spectra and Roughness Indices. *J. Quant. Spectrosc. Radiat. Transf.* **2017**, *200*, 25–31. [CrossRef]
16. Cierniewski, J.; Ceglarek, J.; Kaźmierowski, C. Estimating the Diurnal Blue-Sky Albedo of Soils with given Roughness Using Their Laboratory Reflectance Spectra. *J. Quant. Spectrosc. Radiat. Transf.* **2018**, *217*, 213–223. [CrossRef]
17. Eshel, G.; Levy, G.J.; Singer, M.J. Spectral Reflectance Properties of Crusted Soils under Solar Illumination. *Soil Sci. Soc. Am. J.* **2004**, *68*, 1982. [CrossRef]
18. Goldshleger, N.; Ben-Dor, E.; Benyamini, Y.; Agassi, M. Soil Reflectance as a Tool for Assessing Physical Crust Arrangement of Four Typical Soils in Israel. *Soil Sci.* **2004**, *169*, 677–687. [CrossRef]
19. Thomsen, L.M.; Baartman, J.E.M.; Barneveld, R.J.; Starkloff, T.; Stolte, J. Soil Surface Roughness: Comparing Old and New Measuring Methods and Application in a Soil Erosion Model. *Soil* **2015**, *1*, 399–410. [CrossRef]

20. Monteith, J.L.; Szeicz, G. The Radiation Balance of Bare Soil and Vegetation. *Q. J. R. Meteorol. Soc.* **1961**, *87*, 159–170. [CrossRef]
21. Wang, K.; Liu, J.; Zhou, X.; Sparrow, M.; Ma, M.; Sun, Z.; Jiang, W. Validation of the MODIS Global Land Surface Albedo Product Using Ground Measurements in a Semidesert Region on the Tibetan Plateau. *J. Geophys. Res. Atmos.* **2004**, *109*, D05107. [CrossRef]
22. Oguntunde, P.G.; Ajayi, A.E.; van de Giesen, N. Tillage and Surface Moisture Effects on Bare-Soil Albedo of a Tropical Loamy Sand. *Soil Tillage Res.* **2006**, *85*, 107–114. [CrossRef]
23. Leroy, M.; Deuzé, J.L.; Bréon, F.M.; Hautecoeur, O.; Herman, M.; Buriez, J.C.; Tanré, D.; Bouffiès, S.; Chazette, P.; Roujean, J.L. Retrieval of Atmospheric Properties and Surface Bidirectional Reflectances over Land from POLDER/ADEOS. *J. Geophys. Res. Atmos.* **1997**, *102*, 17023–17037. [CrossRef]
24. Frasner, R.S. Interaction Mechanisms—Within the Atmosphere. In *Manual of Remote Sensing*; American Society of Photogrammetry: Falls Church, VA, USA, 1975; pp. 181–233.
25. Cierniewski, J.; Ceglarek, J.; Karnieli, A.; Ben-Dor, E.; Królewicz, S.; Kaźmierowski, C. Shortwave Radiation Affected by Agricultural Practices. *Remote Sens.* **2018**, *10*, 419. [CrossRef]
26. Cierniewski, J.; Roujean, J.-L.; Jasiewicz, J.; Królewicz, S. Seasonal Net Shortwave Radiation of Bare Arable Land in Poland and Israel According to Roughness and Atmospheric Irradiance. *Remote Sens.* **2021**, *13*, 1897. [CrossRef]
27. Cierniewski, J.; Ceglarek, J.; Kaźmierowski, C.; Roujean, J.L. Combined Use of Remote Sensing and Geostatistical Data Sets for Estimating the Dynamics of Shortwave Radiation of Bare Arable Soils in Europe. *Int. J. Remote Sens.* **2019**, *40*, 2359–2374. [CrossRef]
28. Cierniewski, J.; Ceglarek, J. Annual Dynamics of Shortwave Radiation of Bare Arable Lands on a Global Scale Incorporating Their Roughness. *Environ. Earth Sci.* **2018**, *77*, 777. [CrossRef]
29. Cierniewski, J.; Królewicz, S.; Kaźmierowski, C. Annual Dynamics of Shortwave Radiation as Consequence of Smoothing of Previously Plowed and Harrowed Soils in Poland. *J. Appl. Meteorol. Climatol.* **2017**, *56*, 735–743. [CrossRef]
30. IUSS Working Group WRB. *World Reference Base for Soil Resources 2014. International Soil Classification System for Naming Soils and Creating Legends for Soil Maps*; Food and Agriculture Organization of the United Nations: Rome, Italy, 2014; ISBN 9789251083697.
31. Friedl, M.; Sulla-Menashe, D. MODIS/Terra+Aqua Land Cover Type Yearly L3 Global 0.05Deg CMG V061 [Data Set] 2015. Available online: https://lpdaac.usgs.gov/products/mcd12q1v006/ (accessed on 20 April 2024). [CrossRef]
32. Gorelick, N.; Hancher, M.; Dixon, M.; Ilyushchenko, S.; Thau, D.; Moore, R. Google Earth Engine: Planetary-Scale Geospatial Analysis for Everyone. *Remote Sens. Environ.* **2017**, *202*, 18–27. [CrossRef]
33. Ballabio, C.; Panagos, P.; Monatanarella, L. Mapping Topsoil Physical Properties at European Scale Using the LUCAS Database. *Geoderma* **2016**, *261*, 110–123. [CrossRef]
34. Jasiewicz, J.; Cierniewski, J. SALBEC—A Python Library and GUI Application to Calculate the Diurnal Variation of the Soil Albedo. *Quaest. Geogr.* **2021**, *40*, 95–107. [CrossRef]
35. Allen, R.G.; Pereira, L.S.; Raes, D.; Smith, M. *Crop Evapotranspiration: Guidelines for Computing Crop Requirements*; FAO Irrigation and drainage paper 56; FAO: Rome, Italy, 1998; Volume 285, pp. 19–40.
36. Schneider, S.H.; Dickinson, R.E. Climate Modeling. *Rev. Geophys.* **1974**, *12*, 447. [CrossRef]
37. Kustas, W.P.; Norman, J.M. Use of Remote Sensing for Evapotranspiration Monitoring over Land Surfaces. *Hydrol. Sci. J.* **1996**, *41*, 495–516. [CrossRef]
38. Desjardins, R.L. The Impact of Agriculture on Climate Change. In Proceedings of the 21st annual of the NABC Conference on Adapting Agriculture to Climate Change Symposium, Saskatoon, SK, Canada, 24–26 June 2009; Eagleshham, A., Hardy, R.W.F.A., Eds.; National Agricultural Biotechnology Council: New York, NY, USA; pp. 29–39.
39. Farmer, T.G.; Cook, J. *Climate Change Sicence: A Modern Synthesis. Volume 1—The Physical Climate*; Springer Science & Business Media: Dordrecht, Germany, 2013; ISBN 9780874216561.
40. Mira, M.; Olioso, A.; Gallego-Elvira, B.; Courault, D.; Garrigues, S.; Marloie, O.; Hagolle, O.; Guillevic, P.; Boulet, G. Uncertainty Assessment of Surface Net Radiation Derived from Landsat Images. *Remote Sens. Environ.* **2016**, *175*, 251–270. [CrossRef]
41. Ben-Dor, E.; Ong, C.; Lau, I.C. Reflectance measurements of soils in the laboratory: Standards and protocols. *Geoderma* **2015**, *245–246*, 112–124. [CrossRef]
42. Dent, D.L. ISRIC-World Soil Information. In *Encyclopedia of Soil Science*; Taylor & Francis: Abingdon, UK, 2006; pp. 950–954.
43. Viscarra Rossel, R.A.; Behrens, T.; Ben-Dor, E.; Brown, D.; Demattê, J.; Shepherd, K.; Shi, Z.; Stenberg, B.; Stevens, A.; Adamchuk, V.; et al. A global spectral library to characterize the world's soil. *Earth Sci. Rev.* **2016**, *155*, 198–230. [CrossRef]
44. Sacks, W.J.; Deryng, D.; Foley, J.A.; Ramankutty, N. Crop Planting Dates: An Analysis of Global Patterns. *Glob. Ecol. Biogeogr.* **2010**, *19*, 607–620. [CrossRef]
45. Eurostat Electricity and Heat Statistics. Available online: https://ec.europa.eu/eurostat/statistics-explained/index.php?title=Electricity_and_heat_statistics#Production_of_electricity (accessed on 15 January 2024).